Small-x nuclear shadowing from diffractive scattering

A. Adeluyi and T. Nguyen
Center for Nuclear Research, Department of Physics, Kent State University, Kent, Ohio 44242, USA
(Received 27 February 2007; revised manuscript received 3 April 2007; published 23 May 2007)

We calculate nuclear shadowing ratios at small Bjorken-x for nuclei in the mass range $3 < A < 239$ in the framework of a generalized form of the Gribov theory. The diffractive dissociation cross sections needed as inputs are taken from the FNAL (Fermi National Laboratory) and HERA (Hadron-Electron Ring Accelerator) experiments. Our calculations cover a wide range of energies between 12.8 and 231 GeV. The effects of the inclusion of subleading Reggeons on nuclear shadowing are investigated. At lower energies our results are compared to available data from the New Muon Collaboration (NMC) and E665 Collaboration (E665) experiments at $x \simeq 10^{-4}$. At higher energies subleading Reggeons are found to contribute significantly to nuclear shadowing.

DOI: 10.1103/PhysRevC.75.054911 PACS number(s): 24.85.+p, 25.30.Dh, 25.75.−q, 13.60.Hb

I. INTRODUCTION

Nuclear shadowing is a well-established phenomenon of significant importance to the theoretical description of high energy nucleus-nucleus collisions. In nuclei, for small values of the Bjorken variable $x (x \lesssim 0.1)$, the nuclear structure functions F_2^A are significantly reduced compared to the product of the mass number A and the free nucleon structure function F_2^N. Because the virtual photon-nucleus cross section is proportional to F_2, then equivalently the virtual photon-nucleus cross section is less than A times the one for free nucleons, $\sigma_{\gamma^* A} < A\sigma_{\gamma^* N}$. This phenomenon is generally known as nuclear shadowing in the strict sense. Similar behavior is observed for real photons at sufficiently high energies ($\nu \gtrsim 3$ GeV). Thus the nuclear shadowing ratio, defined as $F_2^A/(A^* F_2^N)$ or alternatively as $\sigma_{\gamma^* A}/(A^*\sigma_{\gamma^* N})$, is less than unity.

The Gribov theory [1], which relates shadowing to diffraction, is an efficacious theoretical framework for understanding nuclear shadowing. For deuteron and other sufficiently light nuclei, the relationship involves the interaction of the diffractively produced hadronic excitations with only two nucleons. In the case of heavier nuclei, triple and higher-order scattering may be important and needs to be included in the formalism. This leads to some model dependence. In the Gribov theory shadowing is expressed in terms of the diffractive dissociation cross section. For low masses of the hadronic excitations, the diffractive dissociation cross section is well described by the vector meson dominance (VMD) model while for higher masses the triple-Regge model is usually employed. The triple-Regge model involves parameters that are not given by the model. These parameters are usually determined from various experimental data on diffraction and photoproduction.

In a previous analysis [2] we used the available data on diffractive dissociation from the Fermi National Laboratory (FNAL) experiment [3] at an average center-of-mass energy $W \simeq 14.3$ GeV. We also restricted the analysis to the triple pomeron contribution of the triple-Regge model. In the present work we use the diffractive dissociation data from both the FNAL experiment at energies $W \simeq 12.8$ GeV and $W \simeq 15.2$ GeV and the experiments at the Hadron-Electron Ring Accelerator (HERA) [4–8] at average energies $W \simeq 187$ GeV and $W \simeq 231$ GeV. Thus the present treatment covers a wider energy range than the previous study. We also investigate the effects of the inclusion of the subleading Reggeons on the description of nuclear shadowing.

As in Refs. [2] and [9] we employ a generalized form of the Gribov theory, incorporating the real part of the diffractive scattering amplitude, to calculate the shadowing ratio at very small Bjorken-x. At applicable energies we compare to experimental results from the New Muon Collaboration (NMC) [10,11] and E665 Collaboration [12,13] experiments. These experimental data are all at small Q^2: thus the use of information from diffractive scattering of real photons ($Q^2 = 0$ GeV^2 at FNAL) and quasi-real photons ($Q^2 < 0.01$ GeV^2 at HERA) is justified.

To present a reasonably self-contained analysis, we include all the relevant details from our previous treatment. The article is thus organized as follows: in Sec. II we review the basic formalism of Gribov theory as applied to shadowing in the small Bjorken-x regime. Section III deals with diffractive production and the diffractive dissociation cross section. These two sections are essentially the same as in the previous analysis. In Sec. IV we describe the data analysis and fits using the triple-Regge model. We present the results of our calculation in Sec. V and conclude in Sec. VI.

II. NUCLEAR SHADOWING AND DIFFRACTION

A. Nuclear shadowing ratio

A high energy (virtual) photon interacting with a nuclear system can experience nuclear effects in two distinct ways [14]:

(i) incoherent scattering from A nucleons with modifications to the structure functions due to many-body effects in the nuclear medium, and
(ii) coherent scattering processes involving more than one nucleon at a time.

Coherence effects occur when hadronic excitations (or fluctuations) produced by the high-energy photon propagate over distances (in the laboratory frame) comparable to or

larger than the characteristic length scale $d \sim 2$ fm. Incoherent scattering manifests primarily in the range $0.1 < x < 1$, while strong coherence effects occur at $x < 0.1$. Shadowing can be understood in terms of coherent scattering on more than one nucleon.

The (virtual) photon-nucleus cross section is separable into a part that accounts for the incoherent scattering from individual nucleons and a correction (shadowing correction) from the coherent interaction with several nucleons:

$$\sigma_{\gamma^* A} = Z\sigma_{\gamma^* p} + (A - Z)\sigma_{\gamma^* n} + \delta\sigma_{\gamma^* A}. \quad (1)$$

The single scattering part is the incoherent sum of photon-nucleon cross sections, where Z is the nuclear charge number and $\sigma_{\gamma^* p}$ and $\sigma_{\gamma^* n}$ are the photon-proton and photon-neutron cross sections, respectively. The multiple scattering correction is expressible as an expansion in the number of nucleons in the target involved in the coherent scattering ($n \geqslant 2$). The dominant contribution to nuclear shadowing comes from double scattering, because the probability that the propagating hadronic excitation coherently interacts with several nucleons decreases with the number of nucleons.

We define the shadowing ratio as

$$\mathcal{R}_A^S = \frac{Z\sigma_{\gamma^* p} + (A - Z)\sigma_{\gamma^* n} + \delta\sigma_{\gamma^* A}}{Z\sigma_{\gamma^* p} + (A - Z)\sigma_{\gamma^* n}}. \quad (2)$$

Thus, the evaluation of the shadowing correction, $\delta\sigma_{\gamma^* A}$, is central to the calculation of the shadowing ratio. We utilize the Gribov theory in a generalized form to determine $\delta\sigma_{\gamma^* A}$ in the next section.

B. Shadowing correction from generalized Gribov theory

We generalize the original formulation of Gribov by including the real part of the diffractive scattering amplitude. We denote by η the ratio of the real to imaginary parts of the diffractive scattering amplitude. In this generalized form incorporating the real part, the shadowing correction at the level of double scattering is given by

$$\delta\sigma_{\gamma^* A} = \frac{A(A-1)}{2A^2} 16\pi \mathcal{R}e \left[\frac{(1 - i\eta)^2}{1 + \eta^2} \times \int d^2b \int_{-\infty}^{\infty} dz_1 \int_{z_1}^{\infty} dz_2 \int_{4m_\pi^2}^{W^2} dM_X^2 \frac{d^2\sigma_{\gamma^* N}^{\rm diff}}{dM_X^2 dt}\bigg|_{t\approx 0} \times \rho_A^{(2)}(\vec{b}, z_1; \vec{b}, z_2) \exp\left\{ i \frac{(z_1 - z_2)}{\lambda} \right\} \right], \quad (3)$$

with $\sigma_{\gamma^* N}^{\rm diff}$ the photon-nucleon diffractive cross section. The coherence length, λ, is given by $\lambda = 2\nu/M_X^2$ for real photons. As illustrated in Fig. 1, a diffractive state with invariant mass M_X is produced in the interaction of the photon with a nucleon located at position $(\vec{b}, z_1)$ in the target. The hadronic excitation is assumed to propagate at fixed impact parameter $\vec{b}$ and to interact with a second nucleon at z_2. The probability to find two nucleons in the target at the same impact parameter is described by the two-body density $\rho_A^{(2)}(\vec{b}, z_1; \vec{b}, z_2)$ normalized as $\int d^3r d^3r' \rho_A^{(2)}(\vec{r}, \vec{r}') = A^2$. The phase factor, $\exp\{i[(z_1 - z_2)/\lambda]\}$, in Eq. (3) implies that only

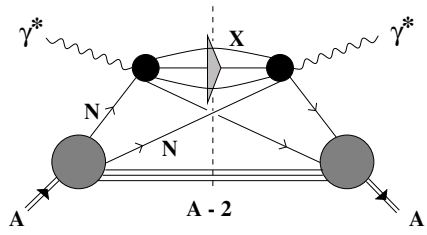

FIG. 1. Double scattering contribution to nuclear DIS.

diffractively excited hadrons with a longitudinal propagation length larger than the average nucleon-nucleon distance in the target, $\lambda > d \simeq 2$ fm, can contribute significantly to double scattering. The limits of integration define the kinematically permitted range of diffractive excitations, with their invariant mass M_X above the two-pion production threshold and limited by the center-of-mass energy $W = \sqrt{s}$ of the scattering process.

We approximate the two-body density $\rho_A^{(2)}(\vec{b}, z_1; \vec{b}, z_2)$ by a product of one-body densities $\rho_A(\vec{r})\rho_A(\vec{r}')$ because short-range nucleon-nucleon correlations are relevant in nuclei only when $z_2 - z_1$ is comparable to the range of the short-range repulsive part of the nucleon-nucleon force, i.e., for distances $\lesssim 0.4$ fm. However, shadowing is negligible in this case and therefore short-range correlations are not important in the shadowing domain.

With increasing photon energies or decreasing x down to $x \ll 0.1$, the longitudinal propagation length of diffractively excited hadrons rises and eventually reaches nuclear dimensions. Thus, for heavy nuclei interactions of the excited hadronic state with several nucleons in the target become important and should be accounted for. Following Ref. [9] we introduce an attenuation factor with an effective hadron-nucleon cross section, $\sigma_{\rm eff}$. The shadowing correction can thus be written as

$$\delta\sigma_{\gamma^* A} = \frac{A(A-1)}{2A^2} 16\pi \mathcal{R}e \left[\frac{(1 - i\eta)^2}{1 + \eta^2} \times \int d^2b \int_{-\infty}^{\infty} dz_1 \int_{z_1}^{\infty} dz_2 \int_{4m_\pi^2}^{W^2} dM_X^2 \frac{d^2\sigma_{\gamma^* N}^{\rm diff}}{dM_X^2 dt}\bigg|_{t\approx 0} \times \rho_A^{(2)}(\vec{b}, z_1; \vec{b}, z_2) \exp\left\{ i \frac{(z_1 - z_2)}{\lambda} \right\} \times \exp\left\{ -(1/2)(1 - i\eta)\sigma_{\rm eff} \int_{z_1}^{z_2} dz \rho_A(b, z) \right\} \right]. \quad (4)$$

The effective hadron-nucleon cross section, $\sigma_{\rm eff}$, in Eq. (4) is defined as

$$\sigma_{\rm eff} = \frac{16\pi}{\sigma_{\gamma N}(1 + \eta^2)} \int_{4m_\pi^2}^{W^2} dM_X^2 \frac{d^2\sigma_{\gamma^* N}^{\rm diff}}{dM_X^2 dt}\bigg|_{t\approx 0}, \quad (5)$$

where $\sigma_{\gamma N}$ is the photon-nucleon cross section. The details of this approach and the approximations inherent in the definition of $\sigma_{\rm eff}$ are treated thoroughly in Ref. [9]. For vector mesons as the intermediate hadronic excitations, we take σ_{VN} as $\sigma_{\rm eff}$ in the attenuation factor in Eq. (4), where σ_{VN} is the vector meson-nucleon scattering cross section.

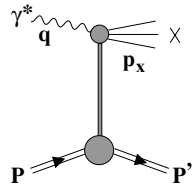

FIG. 2. Diffractive scattering from a proton.

III. DIFFRACTIVE DISSOCIATION

A. Diffractive production

In single diffractive scattering of a (virtual) photon off of a proton (see Fig. 2), the proton remains intact and does not dissociate during the process. The photon, on the other hand, dissociates into a hadronic final state X, with a well-defined rapidity gap relative to the proton.

$$\gamma^{(*)} + p \to X + p'. \tag{6}$$

Such diffractive processes are important at small momentum transfer, with cross sections that decrease exponentially with the squared four-momentum transfer. In general they exhibit a weak energy dependence.

Diffractive dissociation of real photons,

$$\gamma + N \to X + N, \tag{7}$$

has been studied in both fixed target and collider experiments. Experiments were carried out at FNAL at average photon-proton center-of-mass energies of $W \simeq 12.8$ GeV and $W \simeq 15.2$ GeV [3]. Diffractive states with an invariant mass squared of up to $M_X^2 \simeq 18$ GeV^2 were produced. This experiment measured the diffractive dissociation cross section differential in both, the invariant mass M_X and the squared four-momentum transfer t. Experiments at the HERA [4–8] were carried out at average energies $W \simeq 187$ GeV and $W \simeq 231$ GeV. Diffractive states with mass $M_X < 30$ GeV were produced. Unlike the FNAL experiment, only $d\sigma^{\rm diff}_{\gamma^* N}/dM_X^2$ was measured because of poor resolution in t.

As stated in the Introduction, the available experimental data on shadowing at small $x (x \simeq 10^{-4})$ are all at small $Q^2 (Q^2 < 1$ GeV$^2)$. At such small virtualities the photons can be considered quasi-real, and it is thus a reasonable approximation to regard them as real photons with $Q^2 = 0$ GeV^2. The center-of-mass energies are also low: $W \simeq 15$ GeV for the NMC and $W \simeq 25$ GeV for the E665 measurements. The NMC energy ($W \simeq 15$ GeV) is comparable to the photon-proton center-of-mass energy at FNAL ($W \simeq 15.2$ GeV). The E665 energy ($W \simeq 25$ GeV) lies between the FNAL and HERA energies. For these reasons one can use the information from diffractive scattering of real photons at the FNAL and almost real photons ($Q^2 < 0.01$ GeV^2) at the HERA to calculate the shadowing ratio in the kinematic range accessible at NMC and E665. Note that in our previous analysis we used only the FNAL data at $W \simeq 14.3$ GeV. For completeness we also calculate the shadowing ratio at the HERA energies.

B. Diffractive dissociation cross section

The analysis by the H1 collaboration [4] divides the HERA photoproduction data into effectively three intervals in M_X^2. We adopt this approach in the present article, taking the first interval $(0.16 - 1.58)$ GeV^2 to contain the region of the low-mass vector mesons (ρ, ω, and ϕ). The second interval (1.58–4.0 GeV^2) covers the ρ' resonance region. The third interval ($M_X^2 > 4.0$ GeV^2) is that of the high-mass continuum. The differential diffractive cross section is thus written as a sum over contributions from these three mass intervals,

$$\left.\frac{d\sigma^D_{\gamma N}}{dM_X^2 dt}\right|_{t\approx 0} = \sum_{V=\rho,\omega,\phi} \left.\frac{d\sigma^V_{\gamma N}}{dM_X^2 dt}\right|_{t\approx 0} + \sum_{V=\rho'} \left.\frac{d\sigma^V_{\gamma N}}{dM_X^2 dt}\right|_{t\approx 0} + \left.\frac{d\sigma^{\rm cont}_{\gamma N}}{dM_X^2 dt}\right|_{t\approx 0}. \tag{8}$$

In the following, we briefly summarize the various approximations applied in the three regions.

1. Low-mass vector mesons

We utilize the generalized VMD [15] to describe the contribution of the low-mass vector mesons to the differential diffractive cross section, i.e., the first term on the right-hand side of Eq. (8),

$$\left.\frac{d\sigma^V_{\gamma N}}{dM_X^2 dt}\right|_{t\approx 0} = \frac{e^2}{16\pi}\frac{\Pi^V(M_X^2)}{M_X^2}\sigma_{VN}^2, \tag{9}$$

with $\Pi^V(M_X^2)$ the vector meson part of the photon spectral function $\Pi(M_X^2)$, which is given by

$$\Pi(M_X^2) = \frac{1}{12\pi^2}\frac{\sigma(e^+e^- \to \text{hadrons})}{\sigma(e^+e^- \to \mu^+\mu^-)}. \tag{10}$$

In Eq. (9), σ_{VN} is the vector meson-nucleon cross section and $e^2/4\pi = 1/137$ is the fine structure constant. The ω and ϕ mesons are narrow and thus well approximated by δ functions. Their contribution to the photon spectral function can be written as

$$\Pi^V(M_X^2) = \left(\frac{m_V}{g_V}\right)^2 \delta(M_X^2 - m_V^2); \quad V = \omega, \phi, \tag{11}$$

where m_V and g_V ($V = \omega, \phi$) are the mass and the coupling constant of the ω and ϕ mesons, respectively.

The ρ meson, unlike the ω and ϕ mesons, has a large width due to its strong coupling to two-pion states. We have followed the approach in Ref. [16] and taken this into account through the $\pi^+\pi^-$ part of the photon spectral function:

$$\Pi^\rho(M_X^2) = \frac{1}{48\pi^2}\Theta(M_X^2 - 4m_\pi^2) \times \left(1 - \frac{4m_\pi^2}{M_X^2}\right)^{3/2} |F_\pi(M_X^2)|^2, \tag{12}$$

where m_π is the mass of the pion and $M_X = M_{\pi\pi}$ is the invariant mass of the $\pi^+\pi^-$ pair. The pion form factor, F_π, is taken from Ref. [17]. A full discussion is given in Ref. [16].

We compared the result from the δ function approximation to this more exact calculation and found that taking into account the width of the ρ meson increases the differential diffractive cross section by 10%.

The vector meson-nucleon cross section in Eq. (9) has an energy dependence of the form

$$\sigma_{VN} \sim W^{2(\alpha_{\mathbb{P}}(0)-1)} = W^{2\epsilon}, \tag{13}$$

where $\alpha_{\mathbb{P}}(t=0) = 1+\epsilon$ is the soft pomeron intercept [18].

2. Region of the ρ' resonances

The ρ' resonance region contains the $\rho(1450)$ and $\rho(1700)$ mesons. These resonances were formerly classified as the $\rho(1600)$ [19]. The FNAL data show an enhancement in this region. We treat this enhancement in terms of an average ρ' resonance, corresponding to the earlier classification of $\rho(1600)$, as done in Ref. [3]. We use the available information on the $\rho(1600)$ from Ref. [15] in a VMD type calculation to evaluate the contribution from this region. The average ρ' resonance should have a finite width, but encouraged by the fact that a δ function in the case of the ρ gives a good approximation to the full-width result, we employ a narrow resonance approximation for the $\rho(1600)$. Thus, for the second term of (8) we have

$$\left.\frac{d\sigma^V_{\gamma N}}{dM_X^2 dt}\right|_{t\approx 0} = \frac{e^2}{16\pi}\frac{\Pi^V(M_X^2)}{M_X^2}\sigma^2_{VN}, \tag{14}$$

with

$$\Pi^V(M_X^2) = \left(\frac{m_V}{g_V}\right)^2 \delta(M_X^2 - m_V^2) \tag{15}$$

and $V = \rho(1600)$.

3. High-mass continuum

A full treatment of both the FNAL data and the HERA data in this region has been carried out by the H1 Collaboration in Ref. [4], using the triple-Regge model of photon dissociation. Here we limit ourselves to the aspects relevant to the present study. There are two diffractive terms in the triple-Regge expansion: the triple-pomeron ($\mathbb{P}\mathbb{P}\mathbb{P}$) and the pomeron-pomeron-reggeon ($\mathbb{P}\mathbb{P}\mathbb{R}$) terms. The subleading Reggeons have the quantum numbers of the ρ, ω, a_2, and f_2 mesons and their trajectories are approximately degenerate. They are generally referred to as ρ, ω, a, and f mesons and their isospin, signature, and C- and G-parities are $\rho(1--+)$, $\omega(0---)$, $a(1++-)$, and $f(0+++)$, respectively. The pomeron has $\mathbb{P}(0+++)$ and is thus identical to the f meson, leading to interference. We neglect such interference effect in the present study.

The differential dissociation cross section can thus be written as

$$\frac{d^2\sigma}{dM_X^2 dt} = \left[\frac{G_{\mathbb{P}\mathbb{P}\mathbb{P}}(0)}{M_X^{2\alpha_{\mathbb{P}}(0)}} + \frac{G_{\mathbb{P}\mathbb{P}\mathbb{R}}(0)}{M_X^{4\alpha_{\mathbb{P}}(0)-2\alpha_{\mathbb{R}}(0)}}\right] \times (W^2)^{2\alpha_{\mathbb{P}}(0)-2} e^{B(W^2,M_X^2)t}, \tag{16}$$

where $B(W^2, M_X^2) = 2b_{p\mathbb{P}} + 2\alpha'_{\mathbb{P}} ln(W^2/M_X^2)$. Here $b_{p\mathbb{P}}$ is the proton-pomeron slope parameter and $\alpha'_{\mathbb{P}}$ is the slope of the pomeron trajectory. $\alpha_{\mathbb{P}}$ and $\alpha_{\mathbb{R}}$ are the pomeron and (effective) reggeon intercepts, respectively. We use the values in Ref. [4] for these parameters. Note that the value of $\alpha_{\mathbb{P}}(0)$ ($\alpha_{\mathbb{P}}(0) = 1.068 \pm 0.0492$) agrees within error with the soft pomeron intercept in Ref. [18] ($\alpha_{\mathbb{P}}(0) \simeq 1.081$). The triple-pomeron approximation corresponds to putting $G_{\mathbb{P}\mathbb{P}\mathbb{R}}(0) = 0$ in Eq. (16).

IV. DATA ANALYSIS AND FITS

The free parameters to be determined from experimental data are the triple-pomeron coupling $G_{\mathbb{P}\mathbb{P}\mathbb{P}}(0)$ and the pomeron-pomeron-reggeon coupling $G_{\mathbb{P}\mathbb{P}\mathbb{R}}(0)$. We adopt a simple fitting procedure in this article: the experimental data are fitted to Eq. (16) (and the triple-pomeron approximation of it) at the average cms energies. These are $W \simeq 12.8$ GeV and $W \simeq 15.2$ GeV for the FNAL experiment and $W \simeq 187$ GeV and $W \simeq 231$ GeV for the HERA experiment. We first fit the data to the triple-pomeron approximation of Eq. (16), and then, to investigate the effect of the inclusion of the subleading Reggeons, to the full expression in Eq. (16). In the following subsections the units of $G_{\mathbb{P}\mathbb{P}\mathbb{P}}(0)$ and $G_{\mathbb{P}\mathbb{P}\mathbb{R}}(0)$ are μb/GeV$^{2(1+\epsilon)}$ and μb/GeV$^{2(1+\delta)}$ respectively, with $\epsilon = \alpha_{\mathbb{P}}(0) - 1$ and $\delta = \alpha_{\mathbb{R}}(0) - 1$.

A. FNAL data

The FNAL data are presented at $t = -0.05$; thus the data are fitted to Eq. (16) at this value of t. Using the triple-pomeron approximation the fit gives $G_{\mathbb{P}\mathbb{P}\mathbb{P}}(0) = 12.4 \pm 1.8$ for $W \simeq 12.8$ GeV and $G_{\mathbb{P}\mathbb{P}\mathbb{P}}(0) = 10.2 \pm 1.1$ for $W \simeq 15.2$ GeV.

With the full expression Eq. (16), $G_{\mathbb{P}\mathbb{P}\mathbb{P}}(0) = 12.0 \pm 0.4$ and $G_{\mathbb{P}\mathbb{P}\mathbb{R}}(0) = 1.5 \pm 0.1$ at $W \simeq 12.8$ GeV. For $W \simeq 15.2$ GeV, $G_{\mathbb{P}\mathbb{P}\mathbb{P}}(0) = 9.5 \pm 0.7$ and $G_{\mathbb{P}\mathbb{P}\mathbb{R}}(0) = 2.4 \pm 0.3$.

The inclusion of the subleading Reggeons does not have a dramatic effect on the fits. This is because the low M_X^2 region of the continuum is already adequately described by the triple-pomeron contribution. The subleading Reggeons are expected to have appreciable effects at low M_X^2 because their contribution goes like M_X^{-3} and is thus negligible at high M_X^2.

The quality of the fits is shown in Fig. 3.

B. HERA data

The HERA data, unlike the FNAL data, are not presented at a specific value of t. The data have been integrated in t over a kinematic range relevant to the HERA experiment. Thus the first job is to deconvolute the t-integrated data to data at $t = 0$.

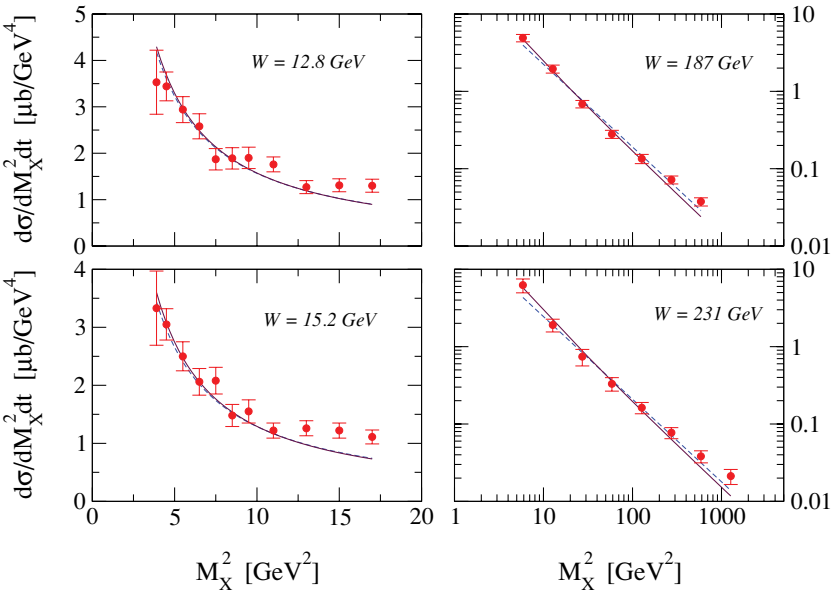

FIG. 3. (Color online) Triple-Regge fit to the FNAL (12.8 GeV and 15.2 GeV) and HERA (187 GeV and 231 GeV) data in the nonresonant continuum ($M_X^2 > 4$ GeV^2). The dashed lines correspond to triple-pomeron only while the thick lines correspond to pomeron+Reggeons. The shaded circles are experimental data.

We assume a t dependence of the form

$$\frac{\mathrm{d}^2\sigma}{\mathrm{d}M_X^2\mathrm{d}t} = \left.\frac{\mathrm{d}^2\sigma}{\mathrm{d}M_X^2\mathrm{d}t}\right|_{t=0} e^{B(W^2,M_X^2)t}, \tag{17}$$

and then integrate both sides of Eq. (17) over the measured range of t, $|t_{\min}| < |t| < 1$ GeV^2. Here $|t_{\min}|$ is the minimum kinematically accessible value of t [19]. In the following equations we suppress the W^2 and M_X^2 dependence of B. We can then write

$$\left.\frac{\mathrm{d}^2\sigma}{\mathrm{d}M_X^2\mathrm{d}t}\right|_{t=0} = \frac{B}{e^{-B|t_{\min}|} - e^{-B}} \int_{|t_{\min}|}^{1} dt \frac{\mathrm{d}^2\sigma}{\mathrm{d}M_X^2\mathrm{d}t}. \tag{18}$$

Making the identification

$$\int_{|t_{\min}|}^{1} dt \frac{\mathrm{d}^2\sigma}{\mathrm{d}M_X^2\mathrm{d}t} \equiv \frac{\mathrm{d}\sigma}{\mathrm{d}M_X^2}, \tag{19}$$

then

$$\left.\frac{\mathrm{d}^2\sigma}{\mathrm{d}M_X^2\mathrm{d}t}\right|_{t=0} = \frac{B}{e^{-B|t_{\min}|} - e^{-B}} \frac{\mathrm{d}\sigma}{\mathrm{d}M_X^2}. \tag{20}$$

Equation (20) can now be applied to generate a new set of data at $t = 0$ from the HERA t-integrated data. With only the triple-pomeron approximation the fit gives $G_{\mathbb{PPP}}(0) = 6.3 \pm 0.7$ for $W \simeq 187$ GeV and $G_{\mathbb{PPP}}(0) = 6.5 \pm 0.6$ for $W \simeq 231$ GeV.

Using the full expression Eq. (16), $G_{\mathbb{PPP}}(0) = 5.0 \pm 0.8$ and $G_{\mathbb{PPR}}(0) = 6.3 \pm 0.8$ at $W \simeq 187$ GeV. For $W \simeq 231$ GeV, $G_{\mathbb{PPP}}(0) = 5.3 \pm 0.8$ and $G_{\mathbb{PPR}}(0) = 8.5 \pm 0.7$.

Here the effect of the inclusion of the subleading Reggeons is apparent. The fits at low M_X^2 are appreciably improved compared with the fits using the triple-pomeron approximation alone. We thus anticipate that the subleading Reggeons will affect the nuclear shadowing ratio substantially at these energies.

The fits are displayed in Fig. 3.

C. $W \simeq 25$ GeV

There are no experimental data at $W \simeq 25$ GeV, the cms energy relevant to the E665 measurements. Thus we are not able to extract both $G_{\mathbb{PPP}}(0)$ and $G_{\mathbb{PPR}}(0)$ directly from experiment. We therefore use an indirect method to estimate these parameters: we plot the fit parameters from Sec. IV A and Sec. IV B as a function of $W^{2(2\alpha_{\mathbb{P}}(0)-2)}$, the energy functional in Eq. (16), and then estimate the values at $W = 25$ GeV. We use the energy functional because it occurs explicitly in the extraction of the fit parameters from experimental data. For the triple-pomeron approximation this approach gives $G_{\mathbb{PPP}}(0) = 8.99 \pm 1.14$. Applying Eq. (16), $G_{\mathbb{PPP}}(0) = 8.04 \pm 0.79$ and $G_{\mathbb{PPR}}(0) = 2.65 \pm 0.32$. This approach, of course, impacts on the accuracy of the determination of the shadowing ratio at this energy because of greater uncertainties associated with the approximate nature of the fit parameters. The fits and corresponding estimates of the fit parameters are are displayed in Fig. 4. Note that $W^{2(2\alpha_{\mathbb{P}}(0)-2)} = W^{0.272}$ using $\alpha_{\mathbb{P}}(0) = 1.068$.

V. RESULTS

The treatment outlined in the last three sections is now applied to calculate the shadowing correction, and hence the shadowing ratio. The basic equation is Eq. (4), which involves the ratio of the real to imaginary amplitudes η, the photon-nucleon cross section $\sigma_{\gamma N}$, the nuclear density ρ_A, and the effective cross section σ_{eff} in terms of the diffractive dissociation cross section.

We use the energy-independent η's for the vector mesons from Ref. [15]. For both ρ and ω mesons, η takes values between 0 and -0.3. Here we take $\eta_\rho = \eta_\omega = -0.2$ in accordance with Ref. [15]. The results of our calculation are not very sensitive to the precise values of $\eta_{\rho(\omega)}$. For the ϕ meson, we take $\eta_\phi = 0.13$ [20]. For lack of information, we take $\eta_{\rho(1600)} = 0$. For the high-mass continuum, we follow

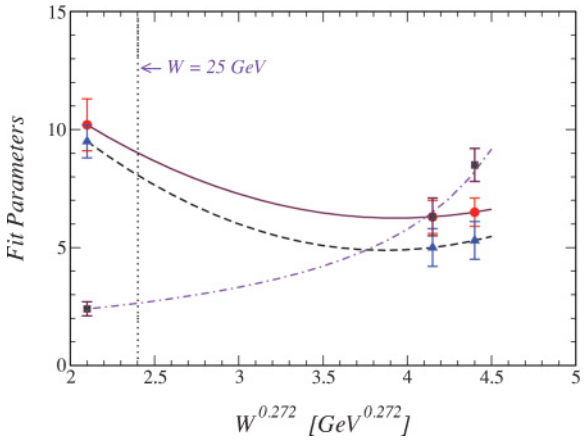

FIG. 4. (Color online) Estimates for the fit parameters at $W = 25$ GeV as discussed in the text. The shaded circles are $G_{\mathbb{PPP}}(0)$ values from the triple-pomeron approximation. The shaded upright triangles and squares are the $G_{\mathbb{PPP}}(0)$ and $G_{\mathbb{PPR}}(0)$, respectively, from Eq. (16). The thick, dashed, and dot-dashed lines are fits to the parameters, respectively. The vertical dotted line corresponds to the values of these parameters at $W = 25$ GeV.

Ref. [9] and define $\eta_{\mathbb{P}}$ as

$$\eta_{\mathbb{P}} = \frac{\pi}{2}(\alpha_{\mathbb{P}}(0) - 1), \tag{21}$$

using the result of Gribov and Migdal [21]. The ratio of the real to imaginary parts of the subleading exchange amplitude $\eta_{\mathbb{R}}$ is given by

$$\eta_{\mathbb{R}} = -\frac{\xi + \cos(\pi\alpha_{\mathbb{R}}(0))}{\sin(\pi\alpha_{\mathbb{R}}(0))}, \tag{22}$$

with $\xi = \pm 1$ the signature factor of the exchanged reggeon. Using the value of $\alpha_{\mathbb{R}}(0) = 0.55 \pm 0.10$ from Ref. [4], $\eta_{\mathbb{R}}(\xi = -1) = 1.17$ and $\eta_{\mathbb{R}}(\xi = +1) = -0.854$. The analysis in Ref. [4] assumes a single effective trajectory $\alpha_{\mathbb{R}}(t)$ for the four subleading Reggeons; thus $-0.854 \leqslant \eta_{\mathbb{R}} \leqslant 1.17$. Because of the uncertainty in $\alpha_{\mathbb{R}}(0)$ and for reasons of symmetry we take the uncertainty range to be $-1 \leqslant \eta_{\mathbb{R}} \leqslant 1$ as in Ref. [9].

The small difference between the photon-proton cross section $\sigma_{\gamma p}$ and the photon-neutron cross section $\sigma_{\gamma n}$ is neglected in this study. We use the Donnachie-Landshoff parametrization of $\sigma_{\gamma p}$ [18] as the generic photon-nucleon cross section $\sigma_{\gamma N}$. For the nuclear densities three-parameter Fermi (3pF) distributions are applied:

$$\rho(r) = \rho_0 \frac{1 + \omega(r/R_A)^2}{1 + e^{(r-R_A)/d}}, \tag{23}$$

with the parameter values taken from Ref. [22]. For mass numbers $A \lesssim 20$ a harmonic oscillator (HO) density distribution may be more appropriate than the 3pF distribution. For uniformity, we use the 3pF distributions for the whole mass range in light of the fact that uncertainties associated with other parameters are at least comparable.

A. Shadowing around FNAL energies

We carried out calculations at $W = 12.8$ and 15.2 GeV, the cms energies of the FNAL measurements. The results are displayed in Fig. 5. At very small $x(x \simeq 10^{-4})$, NMC has two data points, corresponding to ^{6}Li and ^{12}C. The NMC data at $W \simeq 15$ GeV can be compared with the result of our calculation at $W = 15.2$ GeV because the energies are comparable. In view of the large error bars of the data, the calculations can be said to describe the experimental information adequately well in the applicable mass range. There are no data for comparison at $W = 12.8$ GeV.

The inclusion of the Reggeons has small but discernible effects at both the FNAL energies. At $W = 12.8$ GeV the result from pomeron+Reggeons with $\eta = -1$ is pratically similar to the result from the pomeron only. The result of pomeron+Reggeons at $\eta = 1$ is shifted higher relative to both pomeron only and pomeron+Reggeons with $\eta = -1$. This shift generates a gap that is a measure of the uncertainty of the pomeron+Reggeons calculations. Due to the smallness of the gap the triple-pomeron approximation is quite adequate at this energy. At $W = 15.2$ GeV the pomeron+Reggeons ($\eta = -1$) result is still practically the same as that of the

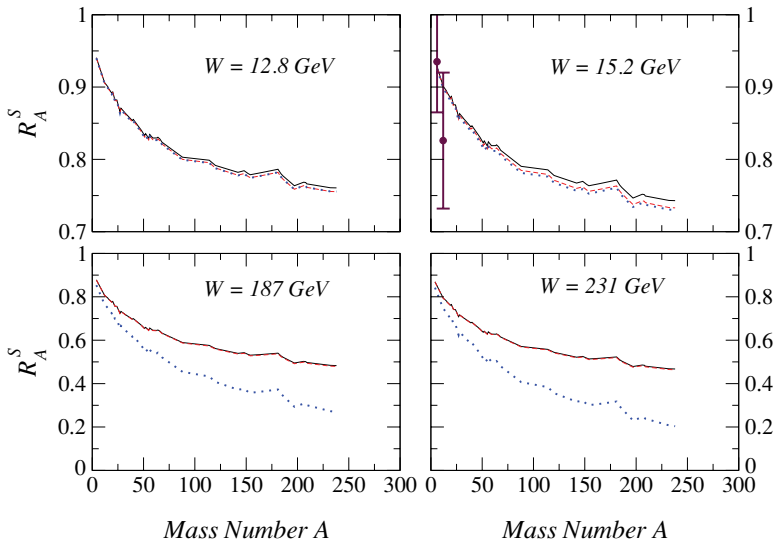

FIG. 5. (Color online) Shadowing ratio at the FNAL and HERA energies. The dots are the results from the triple-pomeron approximation. The thick lines correspond to pomeron+subleading Reggeons with $\eta = 1$ while the dashed lines correspond to pomeron+Reggeons with $\eta = -1$. The shaded circles are data from the NMC experiment.

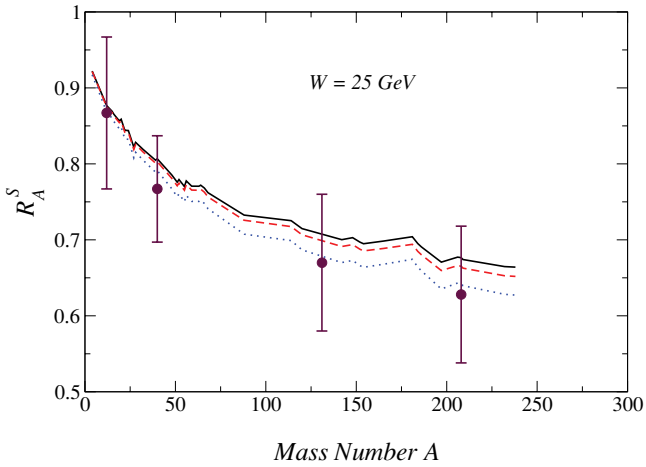

FIG. 6. (Color online) Shadowing ratio at $W = 25$ GeV. The dots are the results from the triple-pomeron approximation. The thick line is the result from both pomeron and subleading Reggeons with $\eta = 1$ while the dashed line corresponds to pomeron+Reggeons with with $\eta = -1$. The shaded circles are data from the E665 experiment.

pomeron only. The gap between the $\eta = 1$ and $\eta = -1$ results is larger, signifying greater uncertainty. Despite the wider gap the triple-pomeron approximation is still also quite good considering the proximity of the results of the pomeron+Reggeons calculations to the triple-pomeron result.

B. Shadowing around $W \simeq 25$ GeV

At very small $x(x \simeq 10^{-4})$ the E665 experiment has four data points: ^{12}C, ^{40}Ca, ^{131}Xe, and ^{208}Pb. The results of our calculations and the experimental data are shown in Fig. 6. The agreement with the experimental result is quite good considering the approximations inherent in the determination of the fit parameters at this energy. For small A the shadowing ratio decreases rapidly with A, while for large A the decrease is more gradual.

The inclusion of the subleading Reggeons has a more appreciable impact at this energy. The effect overall is a lessening of the shadowing correction especially at large A. This results in a greater shadowing ratio compared with the result of the triple-pomeron approximation. Unlike at both $W = 12.8$ and $W = 15.2$ GeV, the result of the pomeron+Reggeons at $\eta = -1$ is clearly different from that of the pomeron alone. A gap similar to that encountered at the FNAL energies exists, with a gap size similar to that at $W = 15.2$ GeV. Because of the difference between the pomeron only and the pomeron+Reggeons results, the inclusion of subleading Reggeons is already becoming important at this energy.

C. Shadowing around HERA energies

Although there are no shadowing data at the HERA energies, it is interesting to see the trend of the shadowing ratio and also the effects of the Reggeons' contributions at these energies. In Fig. 5 we display the results of our calculations at $W = 187$ and 231 GeV. The shapes are identical to the $W = 25$ GeV result: a rapid decrease at small A and a more gradual one as A increases.

The contribution to shadowing from the Reggeons is substantial. As in the previous subsection, the inclusion of the reggeon contribution results in a greater shadowing ratio, with the effect more pronounced at large A. Interestingly, the gap between the pomeron+Reggeons ($\eta = 1$) and the pomeron+Reggeons ($\eta = -1$) results is very small at both energies because the results overlap considerably. Thus the uncertainty from the subleading Reggeons is negligible and the calculations show unambiguously that a proper description of nuclear shadowing around the HERA energies requires the full expression Eq. (16).

D. Comparison with other related approaches

We compare our results to two previous calculations similar in spirit to the present work. In Refs. [14] and [23], Eq. (3) is utilized in an approximately geometrical manner. The real part of the scattering amplitude is neglected and the coherence length λ is taken as infinite. A constant slope parameter B is then used in the expression for the diffractive dissociation cross section. These approximations enable the integral over the diffractive masses to be carried out explicitly yielding the product of the slope parameter B and the nucleonic diffractive cross section $\sigma^{\rm diff}_{\gamma^* N}$. Thus Eq. (3) reduces to a simpler form involving only the integrals over the nuclear densities. Gaussian and square-well parametrizations are used to describe these nuclear densities. The ratio $\sigma^{\rm diff}_{\gamma^* N}/\sigma_{\gamma^* N} \simeq 0.1$ is used with $B \simeq 8$ GeV^{-2}. The calculated results are in good agreement with experimental data from the NMC and E665 experiments and are comparable to the results presented in this study. In contrast to our results at both $W = 15.2$ GeV and $W = 25$ GeV, all the calculated results are below the experimental data points.

The approach in Ref. [24] is slightly different from that adopted in the present study. The basic equation is similar to Eq. (3) but a model form is utilized to describe the diffractive dissociation process. This model form is constructed to describe the HERA data adequately well. As in Refs. [14] and [23], the real part of the amplitude is neglected. The same formalism is adopted in Ref. [25] where two models (Schwimmer and eikonal) are used to account for higher order rescattering effects. Our results are comparable to the $x = 10^{-4}$ ratios of structure functions at $Q^2 = 5.0$ GeV^2 in Ref. [24] and the small-x $Q^2 = 0.5$ GeV^2 structure function ratios in Ref. [25] for the considered nuclei.

E. Uncertainties

The uncertainties of our calculation are directly related to the various uncertainties and approximations inherent in the practical usage of Eq. (4) to determine nuclear shadowing ratio. There are small but finite uncertainties in the nuclear density distribution parameters as well as the neglect of short-range correlations. The parametrizations of the diffractive dissociation cross section in different M_X^2 regions are the dominant sources of uncertainties. In the low-M_X^2 region

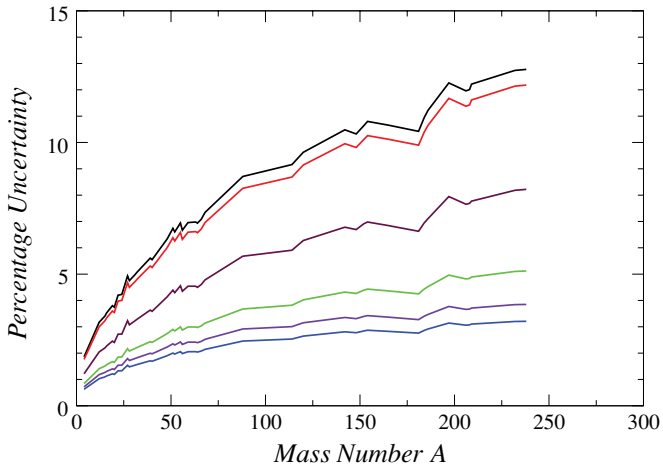

FIG. 7. (Color online) Calculated uncertainties as discussed in the text. From top: $W = 231$ GeV, $W = 187$ GeV, $W = 25$ GeV (triple-pomeron), $W = 25$ GeV, $W = 15.2$ GeV (triple-pomeron), and $W = 15.2$ GeV.

described by the VMD model, the largest contribution to the uncertainties comes from the vector-meson-nucleon cross sections. The δ function parametrization for the ω and ϕ mesons seems adequate, and the width of the ρ meson has been taken into account. Refinements of the spectral function (12) and improvements of the treatment of the ρ' resonance region are possible. In the continuum we have neglected interference between the pomeron and the subleading Reggeons. Also the fit parameters at $W = 25$ GeV are subject to greater errors than the parameters from fits to actual experimental data. Furthermore, the use of an effective scattering cross section to account for multiple scattering is an approximation, as is using real-photon information ($Q^2 = 0$) at small, but non-vanishing Q^2.

Quantitatively, we estimate the overall uncertainty of our calculations as follows: we place a 5% uncertainty on the values of the vector-meson-nucleon cross sections used in the VMD calculations. The uncertainties in the fit parameters are as reported in Sec. IV. From Eq. (4) it can be seen that the uncertainties in the fit parameters propagate into uncertainties in the effective scattering cross section. We have therefore not placed any explicit uncertainty on the effective scattering cross section. We neglect the uncertainties in both $\alpha_{\mathbb{P}}(0)$ and $\alpha_{\mathbb{R}}(0)$ as well as in the other potential sources listed above. Because there are no experimental data in the interval between the FNAL energy (15.2 GeV) and the HERA energy (187 GeV), we place an additional 5% uncertainty on the $W = 25$ GeV fit parameters to offset the lack of constraints on the estimation of these parameters. We use Eq. (16) with $\eta_{\mathbb{R}} = 1$ to estimate the uncertainties at $W = 15.2, 25, 187$, and 231 GeV. For both 187 and 231 GeV the resultant uncertainties represent the total uncertainties because the gaps between $\eta_{\mathbb{R}} = 1$ and $\eta_{\mathbb{R}} = -1$ are negligible. For 15.2 and 25 GeV, the gaps are appreciable and the calculated uncertainties reflect only the uncertainties at $\eta_{\mathbb{R}} = 1$. The $\eta_{\mathbb{R}} = -1$ results are very similar. Since the triple-pomeron approximation is quite good at these two energies, we also estimate the uncertainties using the triple-pomeron approximation of Eq. (16). The percentage uncertainties are diplayed in Fig. 7.

VI. CONCLUSION

Gribov theory, suitably generalized to include the real part of the diffractive scattering amplitude, is employed to calculate the shadowing ratio in nuclei at very small Bjorken-x. We have examined nuclei within the mass range $3 < A < 239$ and for $x \simeq 10^{-4}$. The main input to our calculation, the photon diffractive dissociation cross section, has been parameterized as a function of the invariant mass of the diffractively produced hadronic excitation in three mass intervals. For the low-mass vector mesons and ρ' resonances, the vector meson dominance model is used while the high-mass continuum is treated within the framework of triple-Regge theory. Relevant model parameters are taken from experiments and earlier studies. The calculated shadowing ratio decreases with mass number first rapidly and then more slowly, with stronger decrease with A as the center-of-mass energy increases. The contribution from the subleading Reggeons becomes more substantial as the energy increases. In view of the reasonable agreement of calculated results with experiments at applicable energies, the Gribov theory offers a good description of nuclear shadowing.

[1] V. N. Gribov, Zh. Eksp. Teor. Fiz. **56**, 892 (1969) [Sov. Phys. JETP **29**, 483 (1969)].
[2] A. Adeluyi and G. Fai, Phys. Rev. C **74**, 054904 (2006).
[3] T. J. Chapin *et al.*, Phys. Rev. D **31**, 17 (1985).
[4] C. Adloff *et al.* (H1 Collaboration), Z. Phys. C **74**, 221 (1997).
[5] J. Breitweg *et al.* (ZEUS Collaboration), Eur. Phys. J. C **2**, 237 (1998).
[6] J. Breitweg *et al.* (ZEUS Collaboration), Z. Phys. C **75**, 421 (1997).
[7] S. Aid *et al.* (H1 Collaboration), Z. Phys. C **69**, 27 (1995).
[8] M. Derrick *et al.* (ZEUS Collaboration), Z. Phys. C **63**, 391 (1994).
[9] L. Frankfurt, V. Guzey, and M. Strikman, Phys. Lett. **B586**, 41 (2004).
[10] P. Amaudruz *et al.* (New Muon Collaboration), Nucl. Phys. **B441**, 3 (1995).
[11] M. Arneodo *et al.* (New Muon Collaboration), Nucl. Phys. **B441**, 12 (1995).
[12] M. R. Adams *et al.* (E665 Collaboration), Phys. Rev. Lett. **68**, 3266 (1992).
[13] M. R. Adams *et al.* (E665 Collaboration), Z. Phys. C **67**, 403 (1995).
[14] G. Piller and W. Weise, Phys. Rep. **330**, 1 (2000).
[15] T. H. Bauer, R. D. Spital, D. R. Yennie, and F. M. Pipkin, Rev. Mod. Phys. **50**, 261 (1978) [Erratum, *ibid.* **51**, 407 (1979)].
[16] G. Piller, G. Niesler, and W. Weise, Z. Phys. A **358**, 407 (1997).
[17] F. Klingl, N. Kaiser, and W. Weise, Z. Phys. A **356**, 193 (1996).
[18] A. Donnachie and P. V. Landshoff, Phys. Lett. **B296**, 227 (1992).

[19] K. Hagiwara *et al*. (Particle Data Group), Phys. Rev. D **66**, 010001 (2002).
[20] L. Frankfurt, G. Piller, M. Sargsian, and M. Strikman, Eur. Phys. J. A **2**, 301 (1998).
[21] V. N. Gribov and A. A. Migdal, Sov. J. Nucl. Phys. **8**, 583 (1969) [Yad. Fiz. **8**, 1002 (1968)].
[22] C. W. De Jager, H. De Vries, and C. De Vries, At. Data Nucl. Data Tables **14**, 479 (1974).
[23] G. Piller, L. Ferreira, and W. Weise, Eur. Phys. J. A **4**, 287 (1999).
[24] A. Capella, A. Kaidalov, C. Merino, D. Pertermann, and J. Tran Thanh Van, Eur. Phys. J. C **5**, 111 (1998).
[25] N. Armesto, A. Capella, A. B. Kaidalov, J. Lopez-Albacete, and C. A. Salgado, Eur. Phys. J. C **29**, 531 (2003).